RSC Advances

Advanced removal of toluene in aerosol by adsorption and photocatalytic degradation of silver doped TiO2/PU under visible light irradiation

Journal:	*RSC Advances*
Manuscript ID	RA-ART-11-2015-023786.R1
Article Type:	Paper
Date Submitted by the Author:	19-Jan-2016
Complete List of Authors:	Pham, Thanh-Dong; University of Ulsan, Lee, Byeong-Kyu; University of Ulsan, Pham, Cong De; Pusan National University, Nano Fusion Technology
Subject area & keyword:	Photocatalysis < Catalysis

Advanced removal of toluene in aerosol by adsorption and photocatalytic degradation of silver doped TiO_2/PU under visible light irradiation

Thanh-Dong Pham [a], Byeong-Kyu Lee [a], De Pham-Cong [b]

[a] *Department of Civil and Environmental Engineering, University of Ulsan, Daehakro 93, Namgu, Ulsan 680-749, Republic of Korea*

[b] *Department of Nano Fusion Technology, Pusan National University, Busan 609-735, Republic of Korea*

Corresponding Author: Byeong-Kyu Lee, Professor, Department of Civil and Environmental Engineering, University of Ulsan, Daehakro 93, Namgu, Ulsan, Korea

Tel: 82-52-259-2864, Fax: 82-52-259-2629, E-mail: bklee@ulsan.ac.kr,

Abstract

We synthesized a novel Ag-TiO_2/PU material for the effective removal of gaseous toluene by both adsorption and photocatalytic degradation. The Ag particles, which distributed on the TiO_2 surface, and the Ag dopants, which incorporated into the TiO_2 lattice, increased the electron-hole pair separation efficiency of TiO_2. Therefore, Ag-TiO_2/PU exhibited high photocatalytic degradation of toluene even under visible light. Porous polyurethane (PU) was used to immobilize the enhanced TiO_2, to increase the adsorption capacity of the photocatalyst. The synthesized Ag-TiO_2/PU removed gaseous toluene even under dark condition via adsorption. The removal of gaseous toluene by Ag-TiO_2/PU under visible light conditions was due to the combination of both adsorption and photocatalytic degradation. The oxygen content in the gas stream insignificantly affected the toluene adsorption by the Ag-TiO_2/PU. However, the photocatalytic degradation of toluene by Ag-TiO_2/PU increased with increasing oxygen content and stabilized when the oxygen content exceeded 15 %. These results suggest that ambient air can be used economically as an oxygen source for the photocatalytic degradation of gaseous toluene by Ag-TiO_2/PU under visible light condition. Under visible light irradiation, 6 % Ag-

TiO_2/PU, which was the Ag/TiO_2 ratio that optimized the photocatalytic degradation activity of TiO_2, removed 85.2 % of the toluene in 100ppm inlet gas, of which 90.3 % was mineralized into CO_2 and H_2O.

Keywords: Ag incorporation; toluene removal; photocatalytic degradation; oxygen content effects; visible light

1. Introduction

Many volatile organic compounds (VOCs), emitted from the combustion of fuels, biomass and waste, smoking, solvent use, and the surfaces of carpet, PVC flooring, adhesive products, coating mediums for furniture, and room decorations, have been regulated due to their human toxicity [1, 2]. In particular, even low-dose exposure to carcinogenic benzene and chlorinated VOCs is strongly associated with acute non-lymphocytic leukemia, aplastic anemia and chromosomal aberrations [3]. The inhalation of toluene, which is one of the most commonly found VOCs, can lead to nervous system complications, such as reduction in thinking, memory and muscular abilities, as well as some level of loss in both hearing and color vision [4]. Despite the availability of many treatment technologies, including absorption, condensation, incineration, biological oxidative filtering, and thermal plasma treatment for VOC removal, most have been considered for industrial applications requiring complicated disposal techniques, high costs and skilled labor [5]. Recently, applications for the photocatalytic degradation and removal of gaseous toluene have become a very attractive and promising alternative [6, 7]. Under or near UV irradiation, TiO_2 photocatalyst can photocatalytically degrade toluene into carbon dioxide, water and simple mineral acids [8]. Compared to conventional treatment methods, the use of

photocatalysis for toluene removal exhibited several advantages such as low cost and simplicity [9]. However, the photocatalytic degradation of toluene by TiO_2 photocatalysis is a relative slow process with many limitations for industrial or large-scale application, along with safety issues and high-energy consumption due to UV or near UV irradiation [10].

To overcome these disadvantages, numerous studies have investigated enhancing the photocatalytic activity of TiO_2 and expanding the photocatalytic applications in practical systems using visible or solar irradiation to initiate the photocatalysis [11-15]. Ag has been used as a doping or sensitivity agent to enhance the photocatalytic activity of TiO_2 due to silver's ability to act as both an electron sink and donor to increase the electron-hole pair separation efficiency of TiO_2 and thereby enhance its photocatalytic activity [16]. Due to silver's antibacterial activity, the Ag-doped TiO_2 photocatalyst has been mostly used as a disinfection material [17-20]. A few studies have utilized the synthesized Ag-doped TiO_2 to remove other pollutants, particularly, for removal of toluene gas [21-23]. Thus, the present study firstly aimed to use Ag as a doping agent for enhancing the photocatalytic activity of TiO_2 when applied to the removal of gaseous toluene.

The photocatalytic activity and degradation efficiency, in particular, the degradation of pollutants in gas phase, are strongly dependent on the adsorption capacity of the photocatalyst [24]. Thus, the second aim of the present study was to immobilize TiO_2 and Ag-doped TiO_2 photocatalyst on a polyurethane (PU) substrate, a porous material. We hypothesize that the immobilization and doping would increase the adsorption ability of the photocatalyst for the removal of gaseous toluene. The increased adsorption ability would also increased the degradation rate and hence the toluene removal in aerosol by both adsorption and photocatalytic degradation.

In addition, the photocatalytic degradation processes in aerosol are strongly dependent on the reactions of photo-generated electrons and holes with oxygen and H_2O molecules to produce superoxide radicals ($^{*}O_2^{-}$)and hydroxyl radicals (*OH), respectively [25]. Thus, the moisture and oxygen contents are the key factors affecting the photocatalytic degradation of aerosol pollutants. Several studies have investigated the effects of moisture content on the photocatalytic degradation in aerosol, but without focusing on the effects of oxygen on the degradation [25-29]. Therefore, the third aim of the present study was to investigate the effects of oxygen content on the photocatalytic degradation of toluene in aerosol using Ag-TiO_2/PU under visible light conditions.

2. Materials and Methods

2.1. Synthesis of Ag-TiO_2/PU

Before being used as a substrate to immobilize Ag-doped TiO_2, pristine PU was pre-treated by a mixed solution of toluene, toluene-2,4-diisocyanate, and anhydrous triethylamine to introduce isocyanate groups (NCO) onto its surface [17]. The isocyanated PU was immersed into a solution of amino titanosiloxane, containing a Si-O-Ti bonds and an amine group (NH_2), which was prepared based on reaction between titanium tetraisopropoxide with γ-aminopropyl triethoxysilane. During the immersing process, the titanosiloxane was immobilized on PU by reactions between the isocyanate groups of the isocyanated PU and the amino group (NH_2) of the amino titanosiloxane [17]. After 1 h immersing, the PU immobilized titanosiloxane was taken out and a 0.1 M $AgNO_3$ solution, which was prepared by the dissolution of $AgNO_3$ in deionized water at 60^{o}C, was slowly added (drop-wise) onto the titanosiloxane immobilized on PU. The

obtained material was cleaned using 1 M oxalic acid solution, irradiated with a UV light (60W) for 5 h and calcined under nitrogen at 200°C for 5 h to produce Ag-doped TiO_2 immobilized on PU (Ag-TiO_2/PU). The addition volume of $AgNO_3$ solution was adjusted in order to synthesize Ag-TiO_2/PU materials with Ag/TiO_2 ratios of 0, 2, 4, 6, 8 and 10 wt %.

2.2. Material Characterization

X-ray photoelectron spectroscopy (XPS) spectra of the synthesized Ag-TiO_2/PU materials were obtained using a Thermo Fisher K-Alpha X-ray Photoelectron Spectrometer system. The Gaussian multi-peak shapes were applied to fit the $Ag3d_{5/2}$ and Ti $2p_{3/2}$ peaks in the obtained XPS spectra for determining the elemental state of the silver and titanium in Ag-TiO_2/PU. A Bruker AXN model with a Cu-Kα radiation (λ = 1.5418 Å) source was used to obtain X-ray diffraction (XRD) spectra of Ag-TiO_2/PU. The surface morphology of the Ag-TiO_2/PU materials was analyzed using a Hitachi S-4700 scanning electron microscope (SEM). Before the SEM analysis, the Ag-TiO_2/PU samples were coated with Pt to increase the conductivity of the photocatalyst surface. The surface area (S_{BET}) of the synthesized Ag-TiO_2/PU materials was determined using the Brunauer-Emmett-Teller (BET) isotherm carried out by nitrogen adsorption and desorption at 77K. The optical absorption ability of the Ag-TiO_2/PU materials in the wavelength range 300–700 nm was determined by an Evolution 300 spectrophotometer (UV-1700 Shimadzu).

2.3. Experimental apparatus

Figure 1 shows the experimental apparatus for the continuous photocatalytic degradation and removal of gaseous toluene using Ag-TiO_2/PU. The experimental apparatus was composed of

three main parts: gas generator, reaction chamber and analyzer system. The gas generator system included a mixer, a humidifier and three gas cylinders of 1000ppm toluene in nitrogen gas, oxygen and nitrogen gases (Figure 1). The mixer and humidifier were adjusted to control the toluene gas concentration and humidity level, respectively. The reaction chamber was composed of a dark cover cask (25 x 50 x 50 cm), two 20 W bulbs and a reactor. The bulbs were placed at the top and bottom of the reaction chamber (Figure 1) to generate visible light in the range of 400–700 nm for the photocatalytic irradiation processes. The power density of the generated visible light in the reaction chamber was 0.05 W/cm^2. A reactor (2 x 4 x 15 cm) was placed in the center of the reaction chamber. The top and bottom of the reactor were made of quartz to allow easy passage of the visible light generated from the light bulbs though the reactor wall. The online analyzer system included a Varian CP-3800 gas chromatograph (GC) equipped with a flame ionization detector and a packed column (Porapak Q 80/100 2 x 2 mm) to analyze the concentration of the outlet toluene. A methanizer, using Ni catalyst, was integrated into the GC system to analyze the CO and CO_2 contents in the outlet gas.

2.4. Removal experiments

Flow rate meters were regulated to achieve a constant flow rate of 100 mL/min of 100ppm toluene in the gas mixture. The humidifier was used to ensure that the relative humidity of the gas mixture remained constant at 50 %. Before the toluene removal experiments, the input gas was oriented through direction A to the GC system to re-check the concentration of the toluene in the gas mixture. When the toluene concentration in the 100mL/min flow of mixed gas was stabilized at 100ppm, the input gas was oriented toward direction B where it passed through the reactor volume containing $36cm^3$ of the synthesized Ag-TiO_2/PU porous material. The toluene

142 removal experiments were carried out under conditions of both dark and visible light, achieved
143 by turning the bulbs off/on, respectively, to determine the adsorption and photocatalytic
144 degradation ability of the synthesized Ag-TiO_2/PU, respectively. After the removal experiments,
145 the effluent gas was sent to the GC system using an auto sampling injector, which automatically
146 injected 100 μL of the effluent gas into the packed column in intervals of 10 min from the
147 reaction start time (t_0 =0). The reaction start time (t_0 =0) was estimated to be the time when the
148 input gas was oriented flowing direction B. Helium was used as a carrier gas with a flow rate of
149 25 mL/min. The removal efficiency and mineralization degree of toluene by Ag-TiO_2/PU were
150 evaluated using equations (1) and (2), respectively:

151 $$\text{Toluene removal efficiency } (\%) = \frac{C_0 - C_t}{C_0} \text{x}100\% \quad (1)$$

152 $$\text{Mineralization degree} = \frac{C_{tCO_2}}{7 \times (C_0 - C_t)} \times 100\% \quad (2)$$

153 where:

154 C_0 (100ppm) is the concentration of toluene at the reaction start time (t_0=0), and C_t and C_{tCO2} are
155 the concentrations of toluene and CO_2 at reaction time (t_i=t), respectively.

156

157 **3. Results and Discussion**

158

159 3.1. Material Properties

160 *3.1.1. Elemental States of Silver*

161 The high-resolution XPS spectra of the synthesized Ag-TiO_2/PU indicated that the first
162 elemental state of silver was silver metallic (Ag^0), with peaks at 374.2 and 368.2 eV (Figure 2)
163 [30]. The obtained XRD results further confirmed the existence of Ag^0 on the surface of Ag-

TiO_2/PU (Figure 3) [31]. The Ag^0 was produced from the reduction of $AgNO_3$ under the effects of the UV irradiation and calcination temperature during the Ag-TiO_2/PU preparation processes [16, 32]. The UV irradiation and oxalic acid, rolled as a cleanser for the purification process, enhanced the reduction of $AgNO_3$ into Ag^0 [33-36]. In Ag-TiO_2/PU, silver also existed in form of Ag^+ corresponding to peaks at 373.4 and 367.4 eV in the obtained XPS spectra (Figure 2) [37]. However, the absence of any Ag_2O peak in the XRD spectra (Figure 3) implied that most of the Ag^+ ions had been incorporated into or anchored in the TiO_2 lattice via Ti-O-Ag bonds or that the concentration of Ag^+ existing in form of Ag_2O was too low to be detected by the XRD analysis [21, 32].

The Ag^+/Ag^0 ratios in Ag-TiO_2/PU, which are proportional to the ratios of (the area under the Ag^+ peak)/(the area under the Ag^0 peak) in the XPS spectra, are shown in Table 1. As the Ag/TiO_2 ratio (controlled by increasing the added $AgNO_3$ volume) in Ag-TiO_2/PU was increased to 6 wt %, the Ag^+/Ag^0 ratio increased to a maximum of approximately 55.6%, but then slightly decreased with the further increase of the Ag/TiO_2 ratio above 6 wt %. It was because only a certain amount of Ag^+ could be incorporated into or anchored in the TiO_2 lattice via Ti-O-Ag bonds. At the limitation of the incorporation, the additional Ag^+ in the added $AgNO_3$ could not be further incorporated into the TiO_2 lattice, and was instead reduced into Ag^0 and distributed on the surface of the TiO_2 layer. Thus, the Ag^+/Ag^0ratio slightly decreased as the Ag/TiO_2 ratio was increased above 6 wt %.

3.1.2. Elemental States of Titanium

The obtained XPS results indicate that the elemental state of titanium in TiO_2/PU was only Ti^{4+}, while the elemental states of titanium in the Ag-TiO_2/PU materials were both Ti^{4+} and

Ti^{3+}(Figure 4) [38, 39]. UV irradiation can reduce any Ti^{4+} on the TiO_2 surface to Ti^{3+} [40]. However, the synthesized TiO_2/PU did not contain any Ti^{3+} ions, which indicates that the Ti^{3+} was formed due to the incorporation of silver into the TiO_2 lattice. Atla et al. reported that the incorporated Ag induced a change in the chemical state of TiO_2 leading to the reduction of Ti^{4+} into Ti^{3+} [32]. The incorporation of Ag also induced oxygen vacancies in the TiO_2 lattice, resulting in the reduction of Ti^{4+} to Ti^{3+} [41, 42]. Table 1 shows the calculated Ti^{3+}/Ti^{4+} ratios in the synthesized Ag-TiO_2/PU, which are proportional to the ratios of (the area under the Ti^{3+} peak)/(the area under the Ti^{4+} peak) in the obtained XPS spectra. The results indicate that the Ti^{3+} content in Ag-TiO_2/PU increased rapidly with increasing Ag/TiO_2 ratio, and gradually stabilized when the Ag/TiO_2 ratio rose above 6 wt %. The increase in Ti^{3+} content in Ag-TiO_2/PU was attributed to the increase in Ag content, which was incorporated into the TiO_2 lattice. However, the Ag was only incorporated into the TiO_2 lattice up to a certain limit, leading to the stabilization of Ti^{3+} content in Ag-TiO_2/PU even with the further increase in the Ag/TiO_2 ratio.

3.1.3. Morphology and Surface Area

Figure 5 shows the surface morphology of the synthesized TiO_2/PU, and the 2, 4, 6, 8 and 10% Ag-TiO_2/PU materials. The obtained results indicate that the TiO_2 in TiO_2/PU was smoothly immobilized on the PU surface as a thin layer (Figure 5A). Compared to the surface morphology of TiO_2/PU, the Ag-TiO_2/PU materials exhibited a rougher morphology due to the dispersion of the formed small Ag particles on the surface of the TiO_2 layer. The obtained HRTEM results confirmed the existences of Ag particles on surface of TiO_2 (Figure 6). The lattice spacing of approximately 0.24 and 0.25 nm correspond to the interlayer distance of the (111) and (004) crystal planes Ag [43, 44]. The degree of surface roughness of Ag-TiO_2/PU

increased with increasing Ag/TiO_2 ratio (increasing in Ag particle content). When the Ag/TiO_2 ratios increased up to 8 wt %, the Ag particles began to cluster into larger particles covering the TiO_2 layer.

The BET surface areas of TiO_2/PU and Ag-TiO_2/PU are shown in Table 1. The BET surface area of TiO_2/PU was 110.9 m^2/g, which was much higher than that of commercial TiO_2powder, such as AEROXIDE® TiO_2 P25 obtained from Evonik Degussa Corporation (approximately 60 m^2/g). This indicates that the surface area of $TiO_2$was successfully enhanced by using porous honeycomb PU as a substrate for the immobilization. The obtained BET results also indicate that the surface areas of the synthesized Ag-TiO_2/PU materials were much higher than that of TiO_2/PU. This may have been due to the aforementioned effect of the Ag particles dispersed on the TiO_2 surface in increasing the degree of surface roughness of TiO_2. The BET surface areas of the synthesized Ag-TiO_2/PU materials were also greatly increased with increasing Ag/TiO_2 ratios up to 6 wt %. However, the BET surface area of the areas of the 8 % Ag-TiO_2/PU and 10 % Ag-TiO_2/PU were slightly lower than that of the 6 % Ag-TiO_2/PU. This was attributed to the gathering or cluster of the Ag into larger particles at the high Ag/TiO_2 ratios, according to the SEM analysis. Thus, 6 % Ag-TiO_2/PU exhibited the highest surface area (186.6 m^2/g).

3.1.4. Optical absorption ability

Figure 7 shows the optical absorption in range of 300-700 nm of the synthesized TiO_2/PU and 2, 4, 6, 8 and 10 % Ag-TiO_2/PU materials. TiO_2/PU inherited the optical absorption properties ofTiO_2, which exhibits a strong absorption only in the UV region and the absorption edge around 370nm [13, 45]. The optical absorption of the synthesizedAg-TiO_2/PU materials was observed in both the UV and visible regions. The significant enhancement of optical

absorption in the visible region of Ag-TiO_2/PU was due to a contribution of the plasmon resonance of the Ag particles dispersed onto the TiO_2 surface [46]. The plasmon resonance of Ag particles excited electrons of the valence band of TiO_2 and transferred the excited electrons from the valence band to the conduction band of TiO_2 [45]. The Ag particles also provided sites for the accumulation of the excited electrons, so that Ag acted as an electron sink to hinder the recombination of the excited electrons in the conduction band with holes in the valence band of TiO_2 [47]. Therefore, Ag-TiO_2/PU absorbed the visible light for the separation of the electrons and holes. The light absorption enhancement of Ag-TiO_2/PU was also due to the role of the incorporated Ag, which bonded to TiO_2via Ag-O-Ti bonding, leading to oxygen vacancies and the formation of Ti^{3+} in the TiO_2 lattice. It has been reported that the energy level of Ti^{3+} was located in between the conduction band and the valence band of TiO_2 [47]. Therefore, the formed Ti^{3+} also acted as an intermediate agent to enhance the transfer of electrons from the valence band to the conduction band of TiO_2, contributing to the enhancement of the optical absorption of the synthesized Ag-TiO_2/PU.

Figure 7 also shows that the optical absorption ability of Ag-TiO_2/PU increased as the Ag weight fraction in Ag/TiO_2 increased up to 6 wt %, but then slightly decreased with further increase in the Ag/TiO_2 ratio. At the high Ag/TiO_2 ratios of 8 and 10 wt %, Ag tended to gather into larger particles on the TiO_2 surface (see section 3.1.3), leading to an uneven distribution of Ag particles on the TiO_2 layer or a decrease in the interfacial surface between Ag and TiO_2 (Table 1). Thus, Ag could not act as a more effective electron carrier/sink to enhance the electron hole pair separation efficiency of TiO_2, resulting in the decreased light absorption efficiency of Ag-TiO_2/PU at the high Ag/TiO_2 ratios of 8 and 10 wt %. The large Ag particles also eclipsed the light reaching the TiO_2 surface, thus decreasing the optical absorption of Ag-TiO_2/PU [48].

Thus, a further increase of Ag content in Ag-TiO_2/PU further reduced the light absorption intensity (Figure 7 E and F).

3.2. Toluene Removal

3.2.1. Removal Mechanism

Figure 8 shows the toluene removal results by TiO_2/PU, and 2, 4, 6, 8 and 10% Ag-TiO_2/PU. The experiments were conducted in dark conditions for the first 180 min, after which visible light was provided for an additional 180min. Under the darkened conditions, the outlet toluene concentration gradually increased up to 100ppm at around 165 min, which is the same as the inlet concentration. This means that toluene saturation at the given adsorbent dose (Ag-TiO_2/PU) occurred at around 165 min (Figure 8A). In addition, no CO_2 corresponding to the photocatalytic degradation of gaseous toluene was detected (Figure 8B). This indicates that gaseous toluene was removed solely by adsorption by Ag-TiO_2/PU in darkened conditions. When Ag-TiO_2/PU was exposed to water vapor, its surface was be hydroxylated, leading to the formation of hydroxyl groups on surface of Ag-TiO_2/PU via Ti-OH or Ag-OH bonds [49, 50]. The hydroxyl groups were thus able to bond with the π-electrons of the aromatic ring of toluene, resulting in the adsorption of toluene on the Ag-TiO_2/PU surface [49]. The toluene was also trapped on the Ag-TiO_2/PU surface by physical bond or electrostatic interaction between the aromatic ring of toluene and the various cations, such as Ti^{4+}, Ti^{3+} and Ag^{+}, existing on the Ag-TiO_2/PU surface [51].

Radiation with visible light after saturation did not affect the toluene concentration passing through TiO_2/PU, which indicated that TiO_2/PU did not exhibit any significant photocatalytic

279 degradation activity to remove gaseous toluene under visible light conditions. However, the
280 outlet toluene passing through the Ag-TiO_2/PU materials suddenly increased to a level exceeding
281 the inlet concentration, due to the desorption of the toluene adsorbed on Ag-TiO_2/PU (rolled as
282 an adsorbent) by scrubbing of the CO_2 generated from the photocatalytic degradation of toluene
283 by Ag-TiO_2/PU (mainly acting as a photocatalyst) under visible light conditions. Because the
284 doped Ag enhancing the electron-hole pair generation capacity and separation efficiency of TiO_2,
285 Ag-TiO_2/PU easily generated electron-hole pairs, even under visible. The generated electrons
286 and holes then participated in reactions with the O_2 and/or H_2O molecules in aerosol to produce
287 hydroxyl and superoxide radicals, which are strong oxidative agents. The mechanism by which
288 the hydroxyl and superoxide radicals were generated by Ag-TiO_2/PU under visible light is
289 described by the following reactions:

$$\text{Ag-TiO}_2\text{/PU} \xrightarrow{\textit{Visible light}} e^- + h^+ \quad (3)$$

$$e^- + O_2 \rightarrow + {}^*O_2^- \quad (4)$$

$$h^+ + H_2O \rightarrow H^+ + {}^*OH \quad (5)$$

$$2\,h^+ + 2\,H_2O \rightarrow 2\,H^+ + H_2O_2 \quad (6)$$

$$H_2O_2 \rightarrow 2\,{}^*OH \quad (7)$$

$$36\,{}^*OH + C_7H_8 \rightarrow 7CO_2 + 22\,H_2O \quad (8)$$

290 These generated oxy radicals then participated in the degradation of toluene into CO_2 and
291 H_2O, accompanied by a sharp increase in the CO_2 concentration, as shown in Figure 8B [51-53].
292 The scrubbing of the adsorbed toluene by the CO_2 generated from the photocatalytic degradation
293 of toluene caused desorption of the toluene, which had initially been adsorbed on the Ag-

TiO_2/PU surface during the darkened period. This desorption led to a sudden increase in the toluene concentration in the reactor. Although Ag-TiO_2/PU photocatalytically degraded a certain amount of the toluene passing through the reactor, the outlet toluene rose above its inlet concentration (100 ppm) for a short period before the reaction time reached 255 min. After the adsorbed toluene was almost completely desorbed, the outlet toluene concentration displayed a sharp decrease due to the continuous photocatalytic degradation of toluene by the Ag-TiO_2/PU photocatalyst, accompanied by a decrease in the CO_2 concentration with a slight time lag of around 15 min (Figure 8B). After the adsorbed toluene was almost entirely desorbed, the incoming toluene underwent continuous photocatalytic degradation. Thus, the outlet toluene concentration plateaued in the range of 15 to 38 ppm depending on the Ag content in Ag-TiO_2/PU (Figure 8A).

When visible light was provided from the beginning of the toluene removal experiments (t_0=0), without an adsorption period under dark conditions, the outlet toluene concentrations passing through the Ag-TiO_2/PU materials plateaued at around 10 to 30 ppm after 75 or 90 min (Figure 9A). During the initial experimental period, the toluene was removed by both adsorption and the photocatalytic degradation of Ag-TiO_2/PU. However, the CO_2 gas, generated as a main product of the photocatalytic degradation of toluene, disturbed the adsorption of toluene early on. Thus, if the visible light was provided for longer than 75-90 min, the input toluene was only removed by the photocatalytic degradation activity of Ag-TiO_2/PU.

3.2.2. Optimal Ag content

Figure 8A shows that under dark condition, the slope in the outlet toluene concentration passing through 6% Ag-TiO_2/PU was the shallowest. The steep slope of an adsorption curve is

inversely proportional to the adsorption capacity. A material with a very steep slope in its adsorption curve reaches its adsorption saturation easily or has a low adsorption capacity, whereas a material was a shallower slope has a high adsorption capacity. Thus, among the Ag-TiO_2/PU materials, 6 % Ag-TiO_2/PU exhibited the highest adsorption capacity for toluene removal because it had the highest surface area (Table 1).

Figures 8 and 9 show that the outlet toluene and CO_2 concentrations that passed through the Ag-TiO_2/PU materials under visible light irradiation were stabilized at certain values that could be used to calculate the toluene removal efficiency and the mineralization degree of toluene into CO_2 and H_2O by Ag-TiO_2/PU at different Ag/TiO_2 ratios (Table 2). The toluene removal efficiency and the degree of mineralization by Ag-TiO_2/PU showed similar results for both conditions A and B (explained in the note at the bottom of Table 2). The removal efficiency of toluene increased as the Ag/TiO_2 ratio increased up to 6 wt %, but then gradually decreased with further increase in the ratio. These results were matched by those obtained from the XPS and UV-Vis absorption analyses of Ag-TiO_2/PU photocatalyst. The increase in the Ag/TiO_2 ratio led to an increase in the number of both Ag ions, which were incorporated into the TiO_2 lattice, and metallic Ag, which was dispersed onto the TiO_2 layer. Consequently, the electron-hole separation efficiency and lifespan of the excited electrons in TiO_2 were both increased, which further increased the photocatalytic degradation efficiency of TiO_2. However, the incorporation of Ag ions into the TiO_2 lattice was limited by the tendency of the Ag particles, which had dispersed onto the TiO_2 lattice and thus enhanced the electron-hole pair separation efficiency of TiO_2, to gather into large particles at high Ag/TiO_2 ratios of 8 and 10 wt %, which decreased their enhancement role. Thus, the effect of Ag in enhancing the photocatalytic activity of TiO_2 seemed to reach a limit when the Ag/TiO_2 ratio was 6 wt %.

340

341

342 *3.2.3. Effects of Oxygen content*

343 Figure 10 shows the toluene removal by 6% Ag-TiO_2/PU carried out under darkened
344 conditions for the first 180 min, followed by visible light irradiation for an additional 180 min, as
345 a function of the oxygen content in the input gas stream. Under the darkened condition, the
346 slopes in the outlet toluene concentrations passing through 6 % Ag-TiO_2/PU, and hence its
347 toluene adsorption ability, were not affected by the oxygen content. This indicated that oxygen
348 and toluene were adsorbed at different sites on the Ag-TiO_2/PU surface, so that the adsorption of
349 oxygen did not compete with toluene adsorption [25].

350 Under visible light conditions, the photocatalytic degradation of gaseous toluene using Ag-
351 TiO_2/PU was significantly affected by the oxygen content in the input gas stream. The
352 photocatalytic degradation of toluene increased with increasing oxygen content up to 15 % and
353 then stabilized (Figure 10A). The O_2 reacted with the electrons generated on the surface of Ag-
354 TiO_2/PU to produce superoxide radicals (reaction 4), which increased the photocatalytic
355 degradation of toluene in the gas stream [54]. The reaction between the oxygen and the photo-
356 generated electrons also prevented the recombination of the generated electrons and holes to
357 prolong the lifetime of the generated holes, thereby increasing the production of hydroxyl
358 radicals (via reactions 5 to 7) and hence increasing the degradation of toluene [55]. The reaction
359 between oxygen and electrons peaked at an oxygen content of 15 %, above which the
360 degradation of toluene in the gas stream was stabilized. These study results supported the
361 conclusion that ambient air, with an oxygen content of 21 %, can provide sufficient oxygen for

the economic photocatalytic degradation of gaseous toluene by Ag-TiO_2/PU under visible light condition.

4. Conclusion

The synthesized Ag-TiO_2/PU exhibited high adsorption and photocatalytic degradation for the effective removal of gaseous toluene. The high adsorption ability was attributed to the use of porous PU as a substrate for the immobilization of Ag-TiO_2, which greatly increased the surface area of the adsorbents (Ag-TiO_2/PU). The high photocatalytic degradation of toluene was attributed to the Ag particles, which deposited onto the TiO_2 surface, and the Ag dopants, which incorporated into the TiO_2 lattice. The optimal Ag/TiO_2 ratio for enhancing the photocatalytic degradation activity of $TiO_2$for toluene removal was 6 wt %. Under dark condition, the synthesized Ag-TiO_2/PU exhibited only adsorption activity for removal of gaseous toluene, whereas under visible light irradiation condition it exhibited a combination of both adsorption and photocatalytic degradation. We investigated that the ambient air can be used economically to provide sufficient oxygen for the photocatalytic degradation of gaseous toluene by Ag-TiO_2/PU under visible light condition. Under visible light irradiation, 6 % Ag-TiO_2/PU successfully removed 85.2 % of the 100ppm toluene in gas stream, while 90.3 % of the removed amount was mineralized into CO_2 and H_2O.

Acknowledgments:

This work was supported by a grant from the National Research Foundation of Korea (NRF), funded by the Ministry of Science, ICT and Future Planning (2013R1A2A2A03013138).

Reference

[1] J. Li, S. Lu, G. Liu, Y. Zhou, Y. Lv, J. She, R. Fan, Co-exposure to polycyclic aromatic hydrocarbons, benzene and toluene and their dose–effects on oxidative stress damage in kindergarten-aged children in Guangzhou, China, Science of the Total Environment, 524-525 (2015) 74-80.

[2] H.K. Lai, J.M. Jantunen, N. Kunzli, N. Kulinskaya, R. Colvile, M.J. Nieuwenhuijsen, Determinants of indoor benzene in Europe, Atmospheric Environment, 41 (2007) 9128-9135.

[3] S.N. Sinha, P.K. Kulkarni, S.H. Shah, N.M. Desai, G.M. Patel, M.M. Mansuri, H.N. Saiyed, Environmental monitoring of benzene and toluene produced in indoor air due to combustion of solid biomass fuels, Science of the Total Environment, 357 (2006) 280-287.

[4] A. Rezaee, G.H. Pourtaghi, A. Khavanin, R.S. Mamoory, M.T. Ghaneian, H. Godini, Photocatalytic decomposition of gaseous toluene by TiO_2 nanoparticles coated on activated carbon, Iranian Journal of Environmental Health Science & Engineering, 5 (2008) 305-310.

[5] C. Treesubsuntorn, P. Thiravetyan, Removal of benzene from indoor air by Dracaena sanderiana: Effect of wax and stomata, Atmospheric Environment, 57 (2013) 317-321.

[6] L. Zou, Y. Luo, M. Hooper, E. Hu, Removal of VOCs by photocatalysis process using adsorption enhanced TiO_2–SiO_2 catalyst, Chemical Engineering and Processing, 45 (2006) 959-964.

[7] W.K. Jo, K.H. Park, Heterogeneous photocatalysis of aromatic and chlorinated volatile organic compounds (VOCs) for non-occupational indoor air application, Chemosphere, 57 (2004) 555-565.

[8] W. Chen, J.S. Zhang, UV-PCO device for indoor VOCs removal: Investigation on multiple compounds effect, Building and Environment, 43 (2008) 246-252.

[9] S. Preis, D. Klauson, A. Gregor, Potential of electric discharge plasma methods in abatement of volatile organic compounds originating from the food industry, Journal of Environmental Management, 114 (2013) 125-138.

[10] Z. Han, V.W. Chang, X. Wang, T.T. Lim, L. Hildemann, Experimental study on visible-light induced photocatalytic oxidation of gaseous formaldehyde by polyester fiber supported photocatalysts, Chemical Engineering Journal, 218 (2013) 9-18.

[11] L. Fan, J. Long, Q. Gu, H. Huang, H. Lin, X. Wang, Single-site nickel-grafted anatase TiO_2 for hydrogen production: Toward understanding the nature of visible-light photocatalysis, Journal of Catalysis, 320 (2014) 147-159.

[12] S.N.R. Inturi, T. Boningari, M. Suidan, P.G. Smirniotis, Visible-light-induced photodegradation of gas phase acetonitrile using aerosol-made transition metal (V, Cr, Fe, Co, Mn, Mo, Ni, Cu, Y, Ce, and Zr) doped TiO_2, Applied Catalysis B: Environmental, 144 (2014) 333-342.

[13] B. Wang, G. Zhang, X. Leng, Z. Sun, S. Zheng, Characterization and improved solar light activity of vanadium doped TiO_2/diatomite hybrid catalysts, Journal of Hazardous Materials, 284 (2015) 212-220.

[14] M.B. Fisher, D.A. Keane, Fernández-Ibanez, J. Colreavy, S.J. Hinder, K.G. McGuigan, S.C. Pillai, Nitrogen and copper doped solar light active TiO_2 photocatalysts for water decontamination, Applied Catalysis B: Environmental, 130-131 (2013) 8-13.

[15] T.D. Pham, B.K. Lee, Cu doped TiO_2/GF for photocatalytic disinfection of Escherichia coli in bioaerosols under visible light irradiation: Application and Mechanism, Applied Surface Science, 296 (2014) 15-23.

[16] T.D. Pham, B.K. Lee, Effects of Ag doping on the photocatalytic disinfection of E. coli in bioaerosol by Ag–TiO_2/GF under visible light, Journal of Colloid and Interface Science, 428 (2014) 24-31.

[17] T.D. Pham, B.K. Lee, Novel integrated approach of adsorption and photo-oxidation using Ag-TiO_2/PU for bioaerosol removal under visible ligh, Chemical Engineering Journal, 275 (2015) 357-365.

[18] Y. Jin, Z. Dai, F. Liu, H. Kim, M. Tong, Y. Hou, Bactericidal mechanisms of Ag_2O/TNBs under both dark and light conditions, Water research, 47 (2013) 1837-1847.

[19] G. Xiao, X. Zhang, W. Zhang, S. Zhang, H. Su, T. Tan, Visible-light-mediated synergistic photocatalytic antimicrobial effects and mechanism of Ag-nanoparticles@chitosan–TiO_2 organic–inorganic composites for water disinfection, Applied Catalysis B: Environmental, 170-171 (2015) 255-262.

[20] L. Liu, H. Bai, J. Liu, D.D. Sun, Multifunctional graphene oxide-TiO_2-Ag nanocomposites for high performance water disinfection and decontamination under solar irradiation, Journal of Hazardous Materials, 261 (2013) 214-223.

[21] N. Attarchia, M. Montazer, T. Toliyat, Ag/TiO_2/ β-CD nano composite: Preparation and photo catalytic properties for methylene blue degradation, Applied Catalysis A: General, 467 (2013) 107-116.

[22] C. Liua, C. Cao, X. Luo, S. Luo, Ag-bridged Ag_2O nanowire network/TiO_2 nanotube array p–n heterojunction as a highly efficient and stable visible light photocatalyst, Journal of Hazardous Materials, 285 (2015) 319-324.

[23] D.M. Tobaldi, R.C. Pullar, A.F. Gualtieri, M.P. Seabra, J.A. Labrincha, Sol–gel synthesis, characterisation and photocatalytic activity of pure, W-, Ag- and W/Ag co-doped TiO_2 nanopowders, Chemical Engineering Journal, 214 (2013) 364-375.

[24] R. Djellabi, M.F. Ghorab, G. Cerrato, S. Morandi, S. Gatto, V. Oldani, A.D. Michele, C.L. Bianchi, Photoactive TiO_2–montmorillonite composite for degradation of organic dyes in water, Journal of Photochemistry and Photobiology A: Chemistry, 295 (2014) 57-63.

[25] Y.T. Lin, C.H. Weng, F.Y. Chen, Key operating parameters affecting photocatalytic activity of visible-light-induced C-doped TiO_2 catalyst for ethylene oxidation, Chemical Engineering Journal, 248 (2014) 175-183.

[26] J.F. Wu, C.H. Hung, C.S. Yuan, Kinetic modeling of promotion and inhibition of temperature on photocatalytic degradation of benzene vapor, Journal of Photochemistry and Photobiology A: Chemistry, 170 (2005) 299-306.

[27] X. Fu, L.A. Clark, W.A. Zeltner, M.A. Anderson, Effects of reaction temperature and water vapor content on the heterogeneous photocatalytic oxidation of ethylene, Journal of Photochemistry and Photobiology A: Chemistry, 97 (1996) 181-186.

[28] K. Demeestere, J. Dewulf, B. De Witte, H. Van Langenhove, Titanium dioxide mediated heterogeneous photocatalytic degradation of gaseous dimethyl sulfide: Parameter study and reaction pathways, Applied Catalysis B: Environmental, 60 (2005) 93-106.

[29] C. Raillard, V. Héquet, P.L. Cloirec, J. Legrand, TiO_2 coating types influencing the role of water vapor on the photocatalytic oxidation of methyl ethyl ketone in the gas phas, Applied Catalysis B: Environmental, 59 (2005) 213-220.

[30] A. Amarjargal, L.D. Tijing, H.K. Shon, C.H. Park, C.S. Kim, Facile in situ growth of highly monodispersed Ag nanoparticles on electrospun PU nanofiber membranes: Flexible and high

efficiency substrates for surface enhanced Raman scattering, Applied Surface Science 308, 308 (2014) 396-401.

[31] X. Gao, M. Zhao, Z. Zhang, C. Chen, J. Ma, J. Lu, Effects of hydrogen annealing on the microstructure and optical properties of single-phased Ag_2O film deposited using direct-current reactive magnetron sputtering, Thin Solid Films, 519 (2011) 6620-6623.

[32] S.B. Atla, C.C. Chen, C.Y. Chen, P.Y. Lin, W. Pan, K.C. Cheng, Y.M. Huang, Y.F. Chang, J.S. Jean, Visible light response of Ag^+/TiO_2–Ti_2O_3 prepared by photodeposition under foam fractionation, Journal of Photochemistry and Photobiology A: Chemistry, 236 (2012) 1-8.

[33] Z. Zhang, J.B. Yi, J. Ding, L.M. Wang, H.L. Seng, S.J. Wang, J.G. Tao, G.P. Li, G.Z. Xing, T.C. Sum, C.H.A. Huan, T. Wu, Cu doped ZnO nanoneedles and nanonails:morphological evolution and physical properties Journal of Physical Chemistry C, 112 (2008) 9579-9585.

[34] Q.D. Truong, M. Kakihana, Hydrothermal growth of cross-linked hyperbranched copper dendrites using copper oxalate complex, Journal of Crystal Growth, 348 (2012) 65-70.

[35] E. Morrison, D. Gutiérrez-Tauste, C. Domingo, E. Vigil, J.A. Ayllón, One step room temperature photodeposition of Cu/TiO_2 composite films and its conversion to CuO/TiO_2, Thin Solid Films, 517 (2009) 5621-5624.

[36] A. Kubacka, M.J. Munoz-Batista, M. Fernández-García, S. Obregón, G. Colón, Evolution of H_2 photoproduction with Cu content on CuO_x-TiO_2 composite catalysts prepared by a microemulsion method, Applied Catalysis B: Environmental, 163 (2015) 214-222.

[37] M.H. Ahmed, T.E. Keyes, J.A. Byrne, The photocatalytic inactivation effect of Ag–TiO_2 on β-amyloid peptide (1–42), Journal of Photochemistry and Photobiology A: Chemistry, 254 (2013) 1-11.

[38] H.W.P. Carvalhoa, A.P.L. Batistab, P. Hammer, T.C. Ramalho, Photocatalytic degradation of methylene blue by TiO_2–Cu thin films: Theoretical and experimental study, Journal of Hazardous Materials, 184 (2010) 273–280.

[39] C.S. Kim, J.W. Shin, Y.H. Cho, H.D. Jang, H.S. Byun, T.O. Kim, Synthesis and characterization of Cu/N-doped mesoporous TiO_2 visible light photocatalysts, Applied Catalysis A: General, 455 (2013) 211-218.

[40] H. Liu, W. Yang, Y. Ma, Y. Cao, J. Yao, J. Zhang, T. Hu, Synthesis and characterization of titania prepared by using a photoassisted sol-gel method, Langmuir, 19 (2003) 3001-3005.

[41] R. Jaiswal, N. Patel, D.C. Kothari, A. Miotello, Improved visible light photocatalytic activity of TiO_2 co-doped with Vanadium and Nitrogen, Applied Catalysis B: Environmental, 126 (2012) 47-54.

[42] M. Gurulakshmi, M. Selvaraj, A. Selvamani, P. Vijayan, N.R.S. Rekha, K. Shanthi, Enhanced visible-light photocatalytic activity of V_2O_5/S-TiO_2 nanocomposites, Applied Catalysis A: General, 449 (2012) 31-46.

[43] Z.H. Shah, J. Wang, Y. Ge, C. Wang, W. Mao, S. Zhang, R. Lu, Highly enhanced plasmonic photocatalytic activity of Ag/AgCl/TiO_2 by CuO co-catalyst, Journal of Materials Chemistry A, 3 (2015) 3568–3575.

[44] S. Zhang, L. Chen, L. Liu, W. Guo, Y. Yang, Y. Guo, M. Huo, Design of $H_3PW_{12}O_{40}$/TiO_2 and Ag/$H_3PW_{12}O_{40}$/TiO_2 film-coated optical fiber photoreactor for the degradation of aqueous rhodamine B and 4-nitrophenol under simulated sunlight irradiation, Chemical Engineering Journal, 200-202 (2012) 300-309.

[45] E.S. Aazam, Visible light photocatalytic degradation of thiophene using Ag–TiO_2/multi-walled carbon nanotubes nanocomposite, Ceramics International, 40 (2014) 6705-6711.

519 [46] K.P.O. Mahesh, D.H. Kuo, B.R. Huang, Facile synthesis of heterostructured Ag-deposited
520 SiO_2@TiO_2 composite spheres with enhanced catalytic activity towards the photodegradation
521 of AB 1 dye, Journal of Molecular Catalysis A: Chemical, 396 (2015) 290-296.
522 [47] L.V. Trandafilovic, R.K. Whiffen, S.D. Brankovic, M. Stoiljkovic, A.S. Luyt, V. Djokovic,
523 ZnO/Ag hybrid nanocubes in alginate biopolymer: Synthesis and properties, Chemical
524 Engineering Journal, 253 (2014) 341-349.
525 [48] W.T. Chen, V. Jovic, D. Sun-Waterhouse, H. Idriss, G.I.N. Waterhouse, The role of CuO in
526 promoting photocatalytic hydrogen production over TiO_2, Internation Journal of Hydrogen
527 Energy, 38 (2013) 15036-15048.
528 [49] F. Zhang, M. Wang, X. Zhu, B. Hong, W. Wang, Z. Qi, W. Xie, J. Ding, J. Bao, S. Sun, C.
529 Gao, Effect of surface modification with H_2S and NH_3 on TiO_2 for adsorption and
530 photocatalytic degradation of gaseous toluene, Applied Catalysis B: Environmental, 170-171
531 (2015) 215-224.
532 [50] T.D. Nguyen-Phan, M.B. Song, H. Yun, E.J. Kim, E.S. Oh, E.W. Shin, Characterization of
533 vanadium-doped mesoporous titania and its adsorption of gaseous benzene. , Applied Surface
534 Science, 257 (2011) 2024-2031.
535 [51] M. Takeuchi, M. Hidaka, M. Anpo, Efficient removal of toluene and benzene in gas phase
536 by the TiO_2/Y-zeolite hybrid photocatalyst, Journal of Hazardous Materials, 237-238 (2012)
537 133-139.
538 [52] b.Y. Lee, S.H. Park, S.C. Lee, M. Kang, S.J. Choung, Decomposition of benzene by using a
539 discharge plasma–photocatalyst hybrid system, Catalysis Today, 93-95 (2004) 769-776.
540 [53] H. Dong, G. Chen, J. Sun, C. Li, Y. Yu, D. Chen, A novel high-efficiency visible-light
541 sensitive Ag_2CO_3 photocatalyst with universal photodegradation performances: Simple

synthesis, reaction mechanism and first-principles study, Applied Catalysis B: Environmental, 134-135 (2013) 46-54.

[54] A.K. Boulamanti, C.J. Philippopoulos, Photocatalytic degradation of methyl tert-butyl ether in the gas-phase: A kinetic study, Journal of Hazardous Materials, 160 (2008) 83-87.

[55] X.V. Doorslaer, P.M. Heynderickx, K. Demeestere, K. Debevere, H.V. Langenhove, J. Dewulf, TiO_2 mediated heterogeneous photocatalytic degradation of moxifloxacin: Operational variables and scavenger study, Applied Catalysis B: Environmental, 111-112 (2012) 150-156.

Table 1: The ratios of Ag^0/Ag^+ and Ti^{3+}/Ti^{4+} and the BET surface area of the Ag-TiO_2/PU materials

	Ag^+/Ag^0 ratios (%)	**Ti^{3+}/Ti^{4+} ratios** (%)	**BET surface area** (m^2/g)
TiO_2/PU	-	0	110.9
2 % Ag-TiO_2/PU	42.4	15.5	129.2
4 % Ag-TiO_2/PU	48.8	19.7	155.7
6 % Ag-TiO_2/PU	55.6	22.6	186.6
8 % Ag-TiO_2/PU	54.3	23.4	176.3
10 % Ag-TiO_2/PU	53.1	24.2	148.1

Table 2: The toluene removal efficiency and the mineralization degree by Ag-TiO_2/PU photocatalysts at different Ag/TiO_2 ratios under visible light conditions

	Condition A		**Condition B**	
	Removal efficiency (%)	Mineralization degree (%)	Removal efficiency (%)	Mineralization degree (%)
2 % Ag-TiO_2/PU	62.5	88.2	62.9	88.5
4 % Ag-TiO_2/PU	68.3	89.1	68.7	89.6
6 % Ag-TiO_2/PU	85.2	90.3	85.6	90.8
8 % Ag-TiO_2/PU	81.4	88.4	81.7	89.1
10 % Ag-TiO_2/PU	75.6	89.3	76.5	88.4

Note: Condition A: Light was provided after the toluene was adsorbed during the darkened period (0-180 min)
Condition B: Light was provided from the beginning of the toluene removal ($t=t_o$).

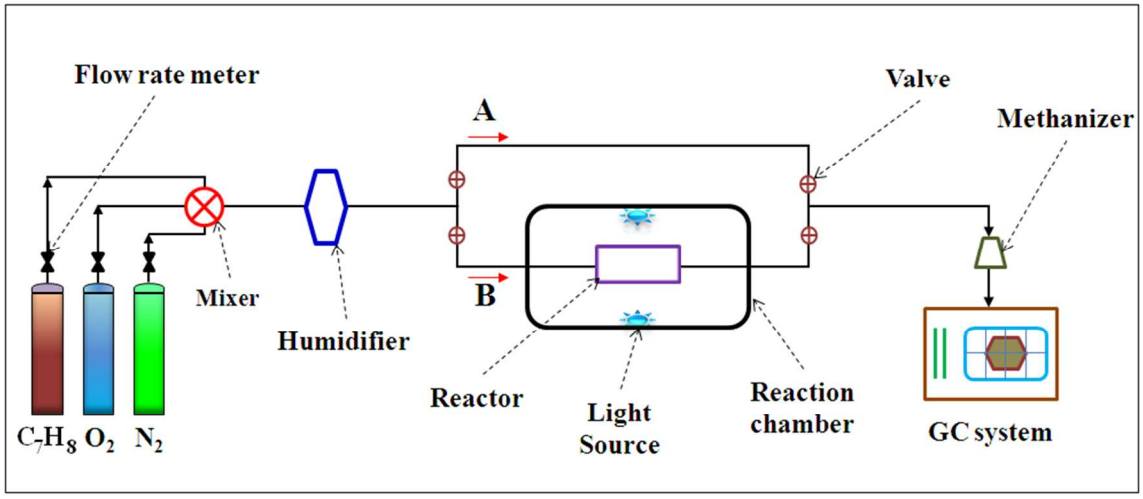

Figure 1: The experimental apparatus for removal of gaseous toluene

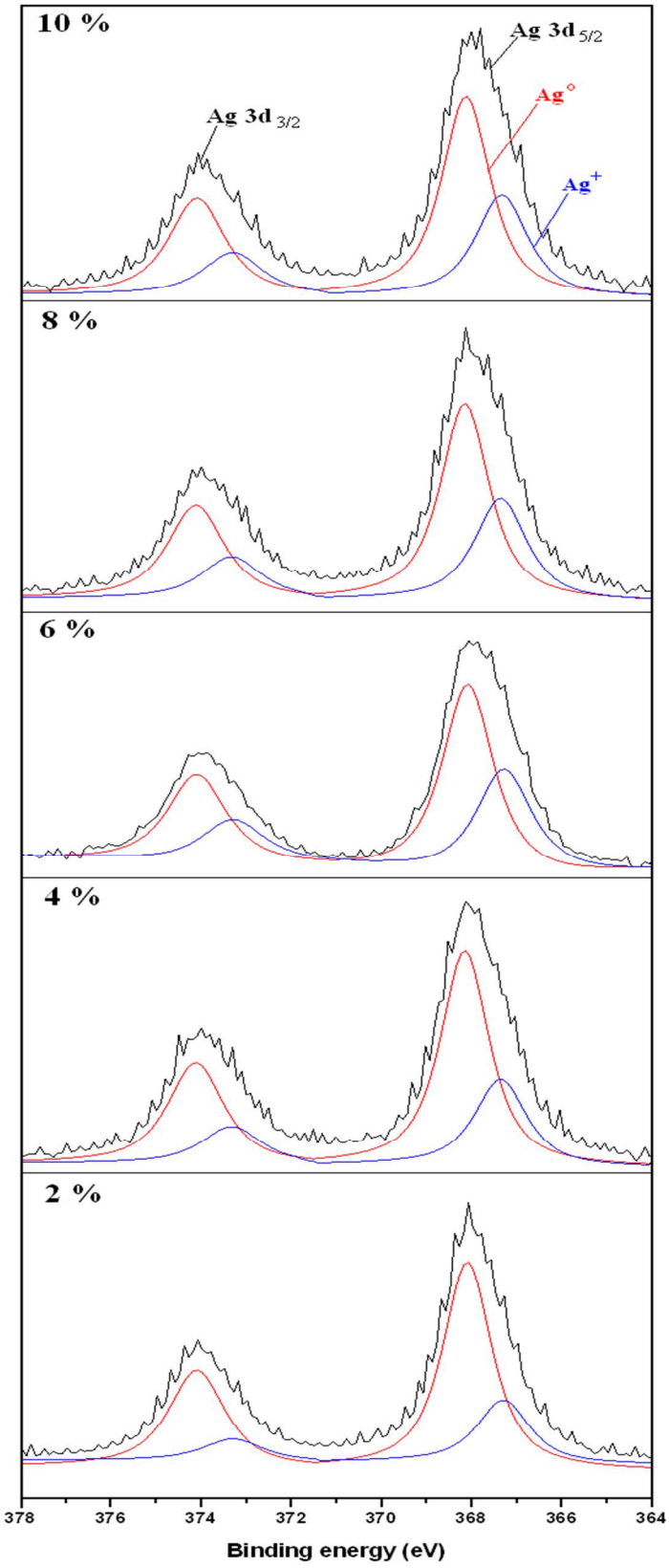

Figure 2: High-resolution XPS spectra of Ag in X % Ag-TiO_2/PU

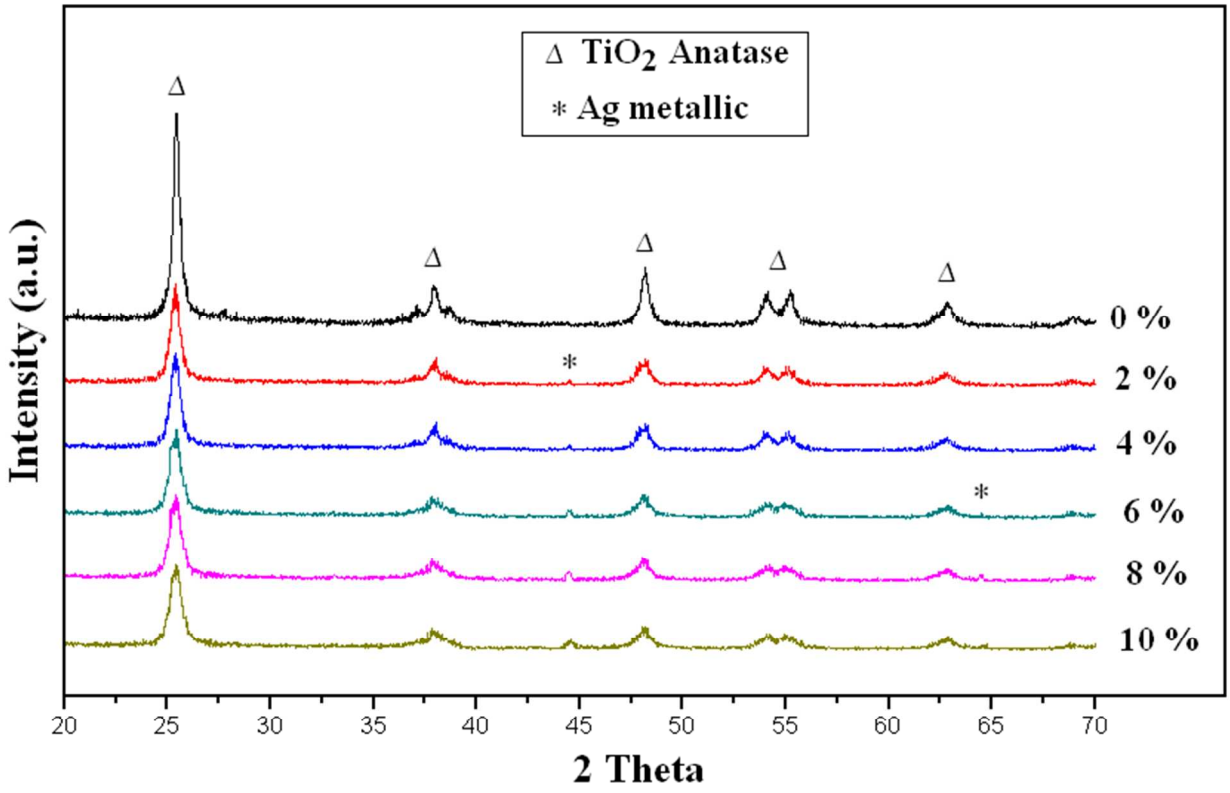

Figure 3: XRD patterns of X % Ag-TiO_2/PU

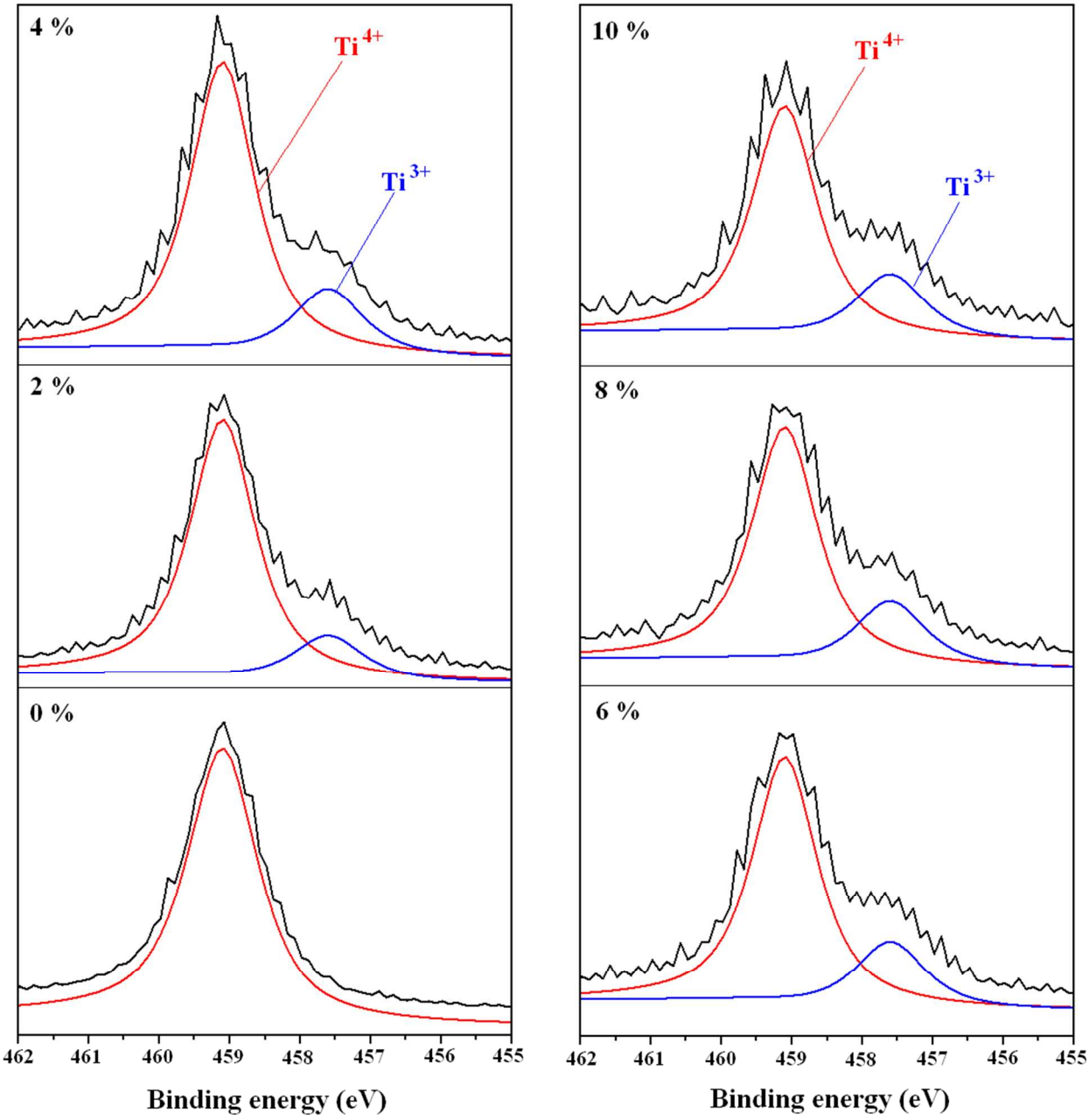

Figure 4: High-resolution XPS spectra of Ti $2p_{3/2}$ in X % Ag-TiO_2/PU

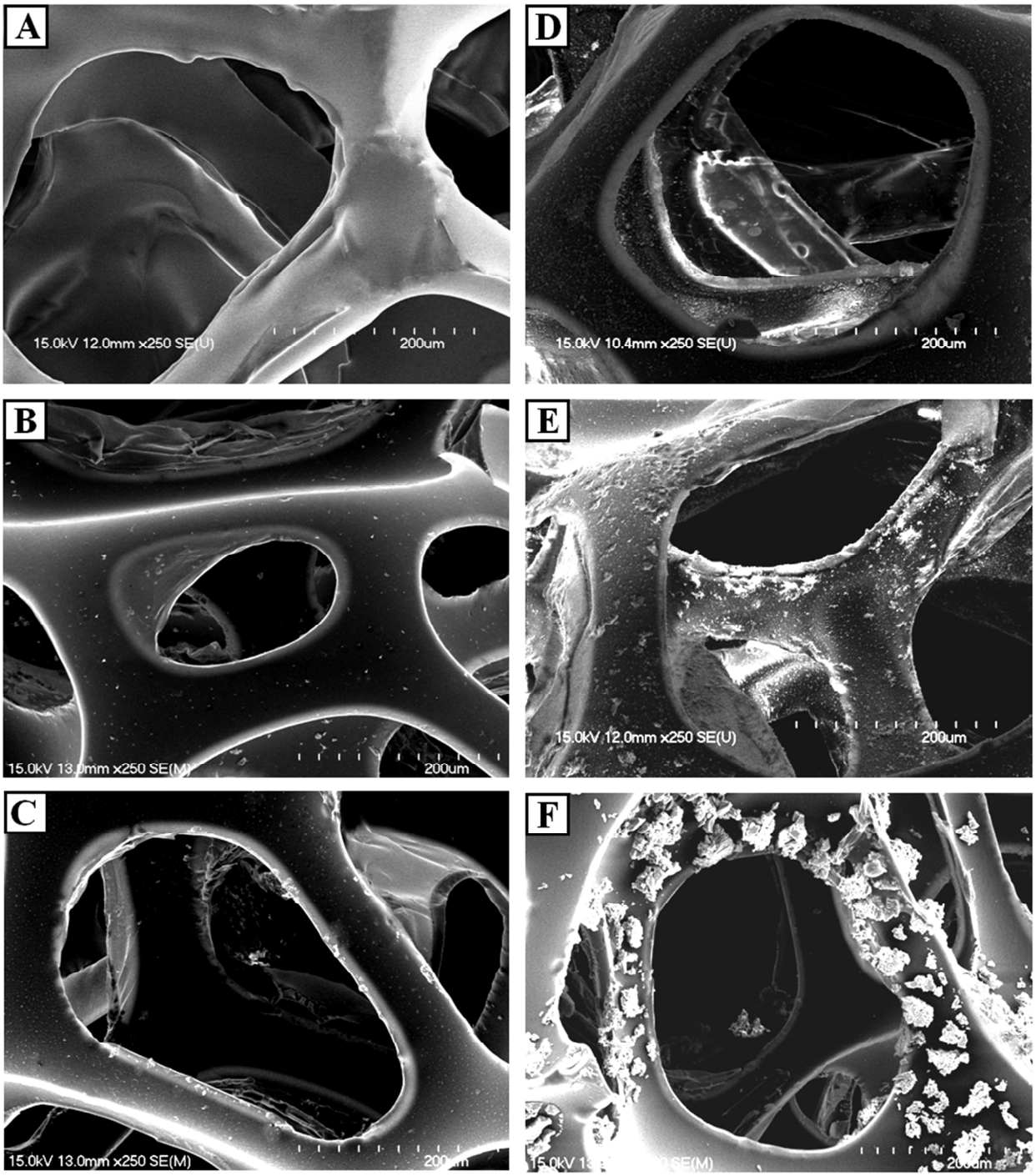

Figure 5: SEM of TiO_2/PU (A), and 2% (B), 4% (C), 6% (D), 8% (E) and 10% (F) Ag-TiO_2/PU

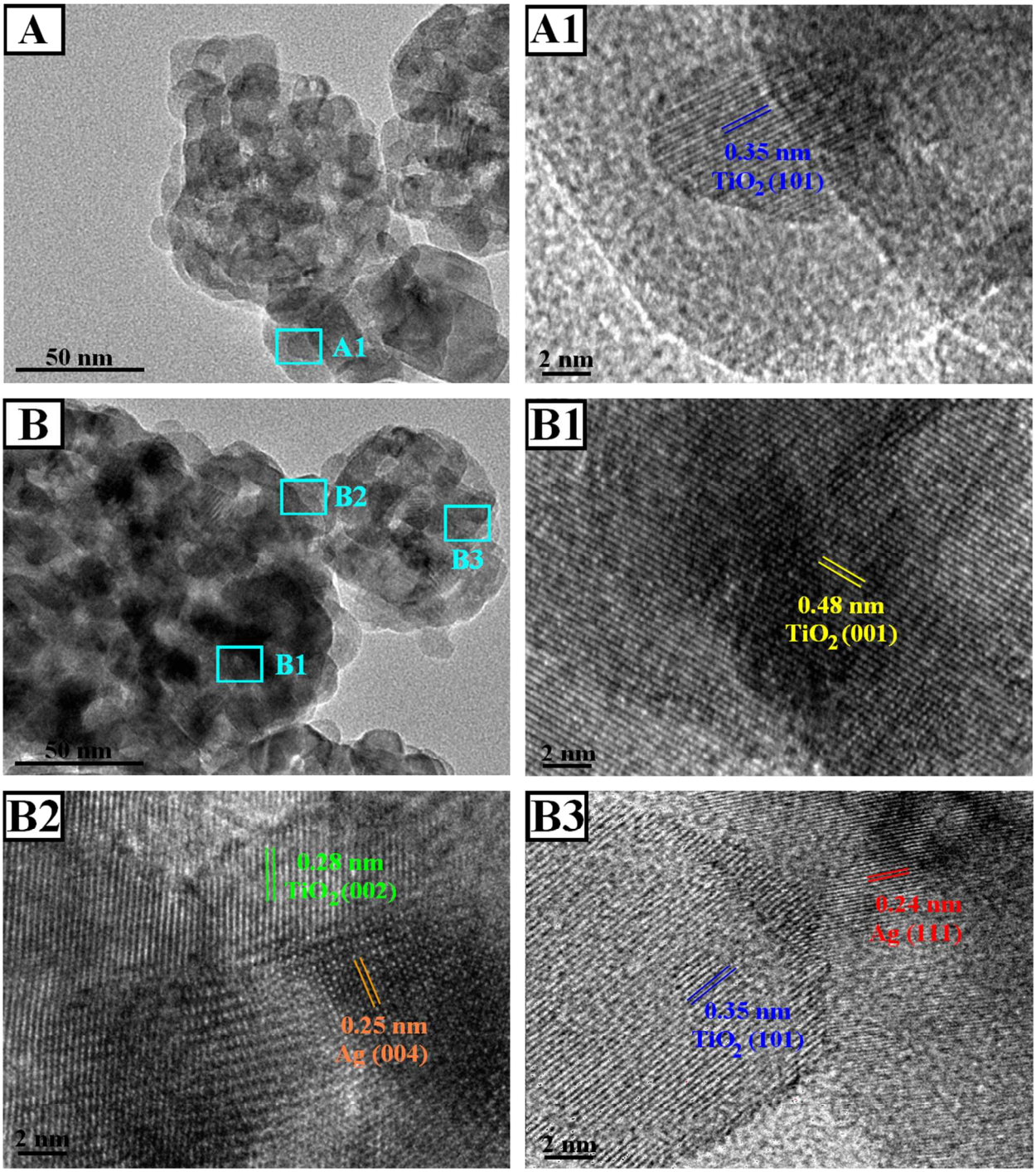

643

644 Figure 6: TEM images of TiO_2/PU (A) and Ag-TiO_2/PU (B); HRTEM images of the selected

645 areas in the TEM images of TiO_2/PU (A1) and Ag-TiO_2/PU (B1, B2 and B3).

646

647

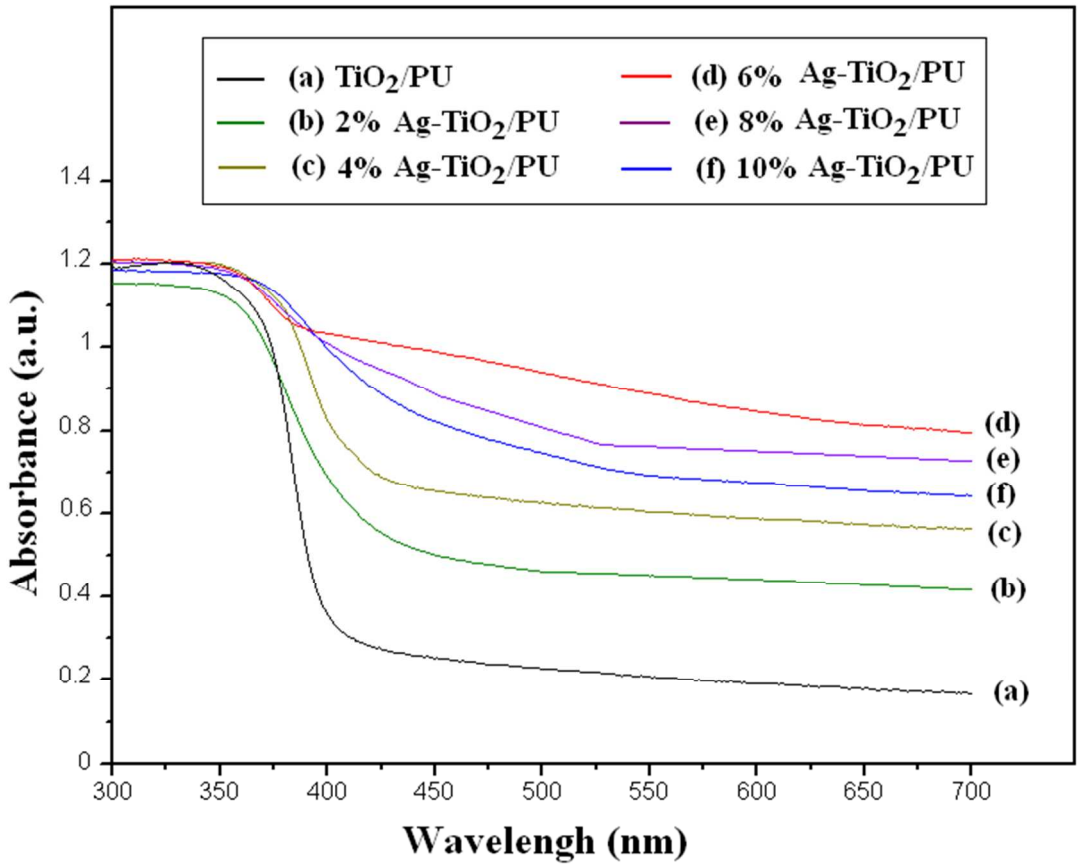

Figure 7: UV-Vis absorption spectra of TiO_2/PU and 2, 4, 6, 8 and 10 % Ag-TiO_2/PU

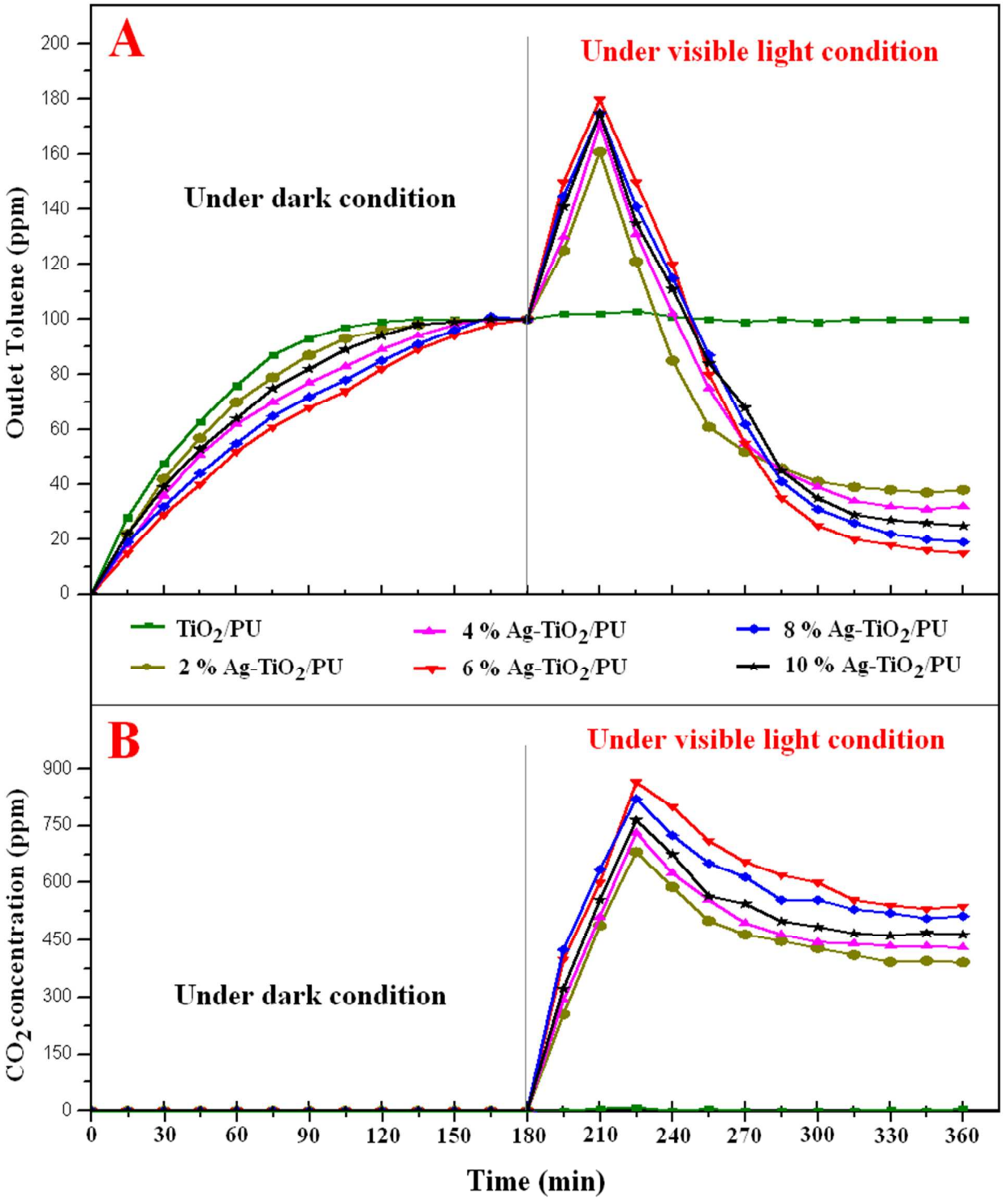

Figure 8: Toluene removal (A) and generated CO_2 concentration (B) by X % Ag-TiO_2/PU under dark and then visible light conditions

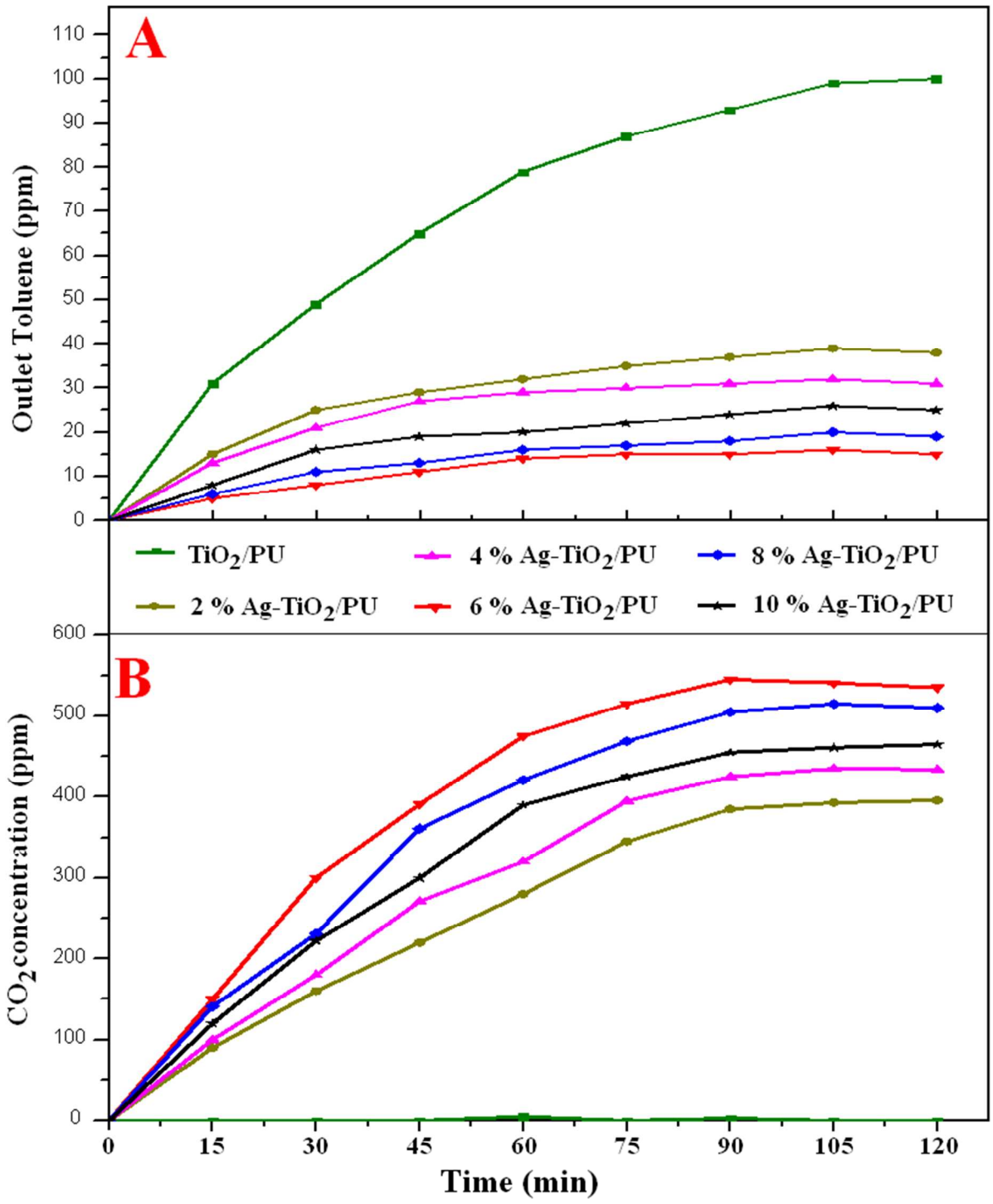

Figure 9: Toluene removal (A) and generated CO_2 concentration (B) by X % Ag-TiO_2/PU under visible light conditions

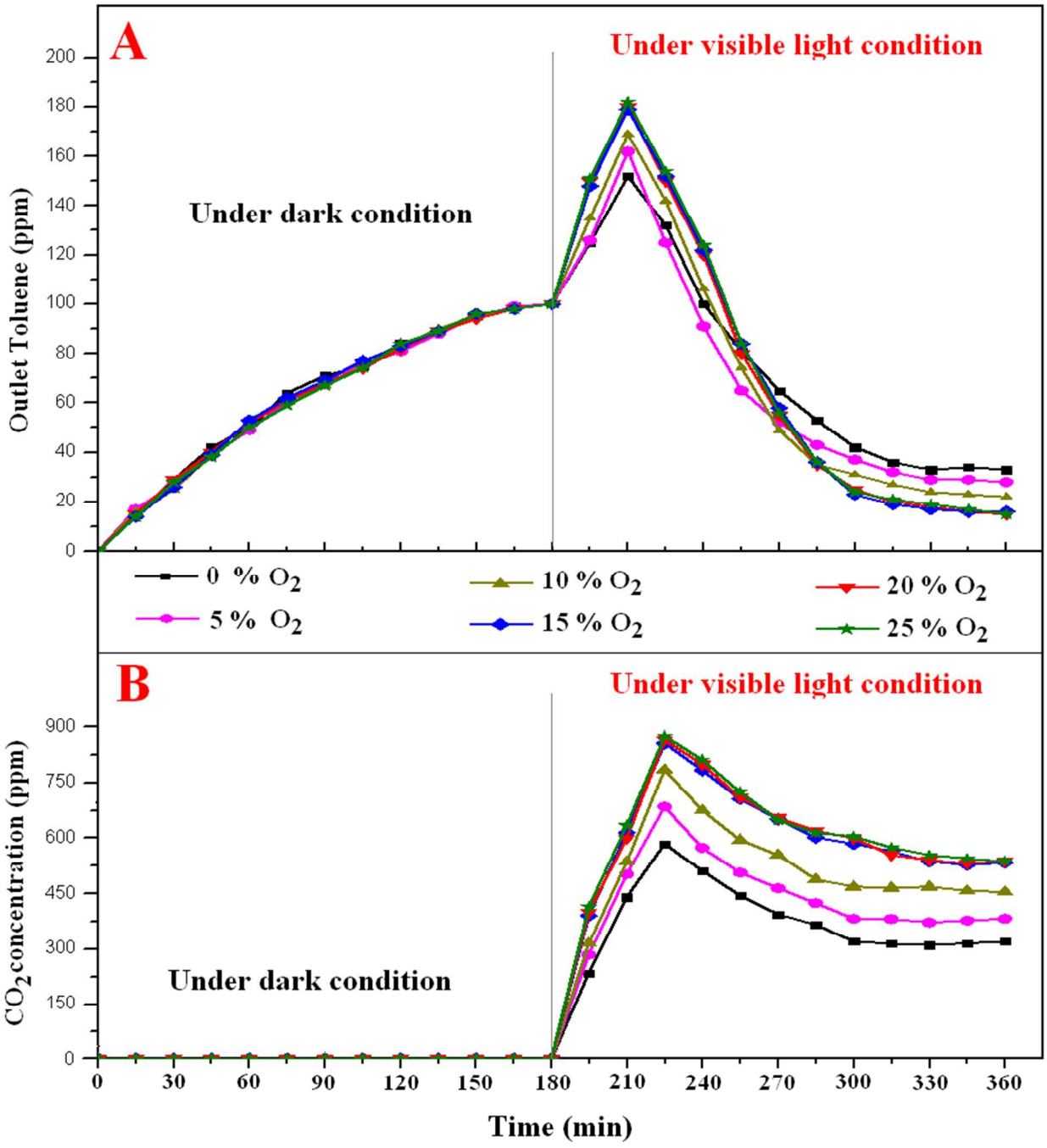

Figure 10: Effect of O_2 content on outlet toluene (A) and generated CO_2 concentration (B) passing 6% Ag-TiO_2/PU

671 **Table captions**

672 Table 1: The ratios of Ag^0/Ag^+ and Ti^{3+}/Ti^{4+} and the BET surface area of the Ag-TiO_2/PU
673 materials

674 Table 2: The toluene removal efficiency and the mineralization degree by Ag-TiO_2/PU
675 photocatalysts at different Ag/TiO_2 ratios under visible light conditions

676

677 **Figure captions**

678 Figure 1: The experimental apparatus for removal of gaseous toluene

679 Figure 2: High-resolution XPS spectra of Ag in X % Ag-TiO_2/PU

680 Figure 3: XRD patterns of X % Ag-TiO_2/PU

681 Figure 4: High-resolution XPS spectra of Ti $2p_{3/2}$ in X % Ag-TiO_2/PU

682 Figure 5: SEM of TiO_2/PU (A), and 2% (B), 4% (C), 6% (D), 8% (E) and 10% (F) Ag-TiO_2/PU

683 Figure 6: TEM images of TiO_2/PU (A) and Ag-TiO_2/PU (B); HRTEM images of the selected
684 areas in the TEM images of TiO_2/PU (A1) and Ag-TiO_2/PU (B1, B2 and B3).

685 Figure 7: UV-Vis absorption spectra of TiO_2/PU and 2, 4, 6, 8 and 10% Ag-TiO_2/PU

686 Figure 8: Toluene removal (A) and generated CO_2 concentration (B) by X % Ag-TiO_2/PU under
687 dark and then visible light conditions

688 Figure 9: Toluene removal (A) and generated CO_2 concentration (B) by X % Ag-TiO_2/PU under
689 visible light conditions

690 Figure 10: Effect of O_2 content on outlet toluene (A) and generated CO_2 concentration (B)
691 passing 6% Ag-TiO_2/PU

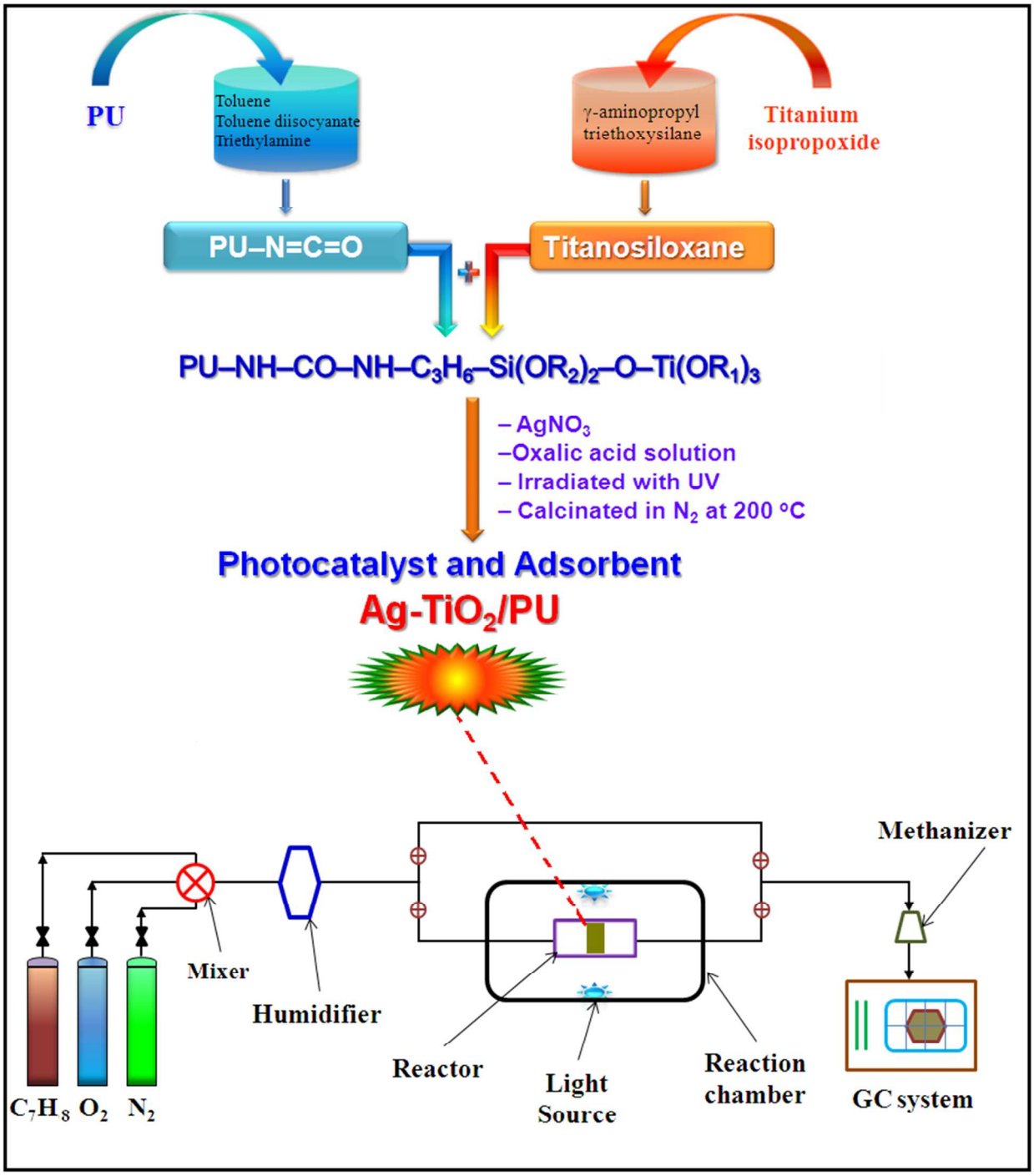
PU
Toluene
Toluene diisocyanate
Triethylamine
γ-aminopropyl triethoxysilane
Titanium isopropoxide
PU–N=C=O
Titanosiloxane
PU–NH–CO–NH–C3H6–Si(OR2)2–O–Ti(OR1)3
– AgNO3
–Oxalic acid solution
– Irradiated with UV
– Calcinated in N2 at 200 °C
Photocatalyst and Adsorbent
Ag-TiO2/PU
Methanizer
Mixer
Humidifier
Reactor
Light Source
Reaction chamber
GC system
C7H8 O2 N2